2025 American Control Conference (ACC)
July 8-10, 2025. Denver, CO, USA

Adaptive Estimation of All-Solid-State Battery Temperatures with Thermal Conductivity Uncertainties

Patryck Ferreira and Shu-Xia Tang

***Abstract*— All-Solid-State Batteries (ASSBs) offer enhanced safety and higher energy density compared to conventional Lithium-ion Batteries (LiBs), but their thermal management is challenging due to time-varying thermal properties. The thermal behavior of ASSBs is modeled by five Ordinary Differential Equations (ODEs) representing the temperatures of the case surface (near the cathode and anode), cathode, electrolyte, and anode. These temperatures are driven by heat from the battery, derived from an electrochemical model using two Partial Differential Equations (PDEs) for Li^+ ions concentration. This study presents an adaptive observer that adjusts thermal conductivities in real-time, accurately estimating ASSB temperatures. Simulations demonstrate that the observer effectively tracks time-varying conductivities, with estimation errors converging to zero and improving thermal management accuracy.**

***Index Terms*— All-Solid-State Batteries, Adaptive Observer, Electrochemical-Thermal Model, Time-Varying Parameters, Thermal Conductivity.**

I. Introduction

ASSBs are a promising advancement in energy storage technology, offering enhanced safety by replacing flammable liquid electrolytes with solid electrolytes, thereby reducing the risk of fire and explosion [1]. This shift not only allows the use of lithium-metal anodes, which increases energy density compared to conventional LiBs, but also introduces challenges related to inefficient cycling behavior and dendrite formation in lithium-metal anodes [2]. These dendrites can penetrate the solid electrolyte, leading to internal short circuits [3]. While ASSBs inherently offer improved safety due to their solid electrolytes compared to LiBs with liquid electrolytes [4], effective thermal management remains critical, especially given the dynamic nature of thermal parameters influenced by aging and operational conditions.

Current models for ASSBs primarily focus on electrochemical processes, with less emphasis on the evolving thermal properties that impact battery performance and safety [5]. Although recent advancements, such as the quintuple thermal model in [6], provide better temperature estimation, they often assume constant thermal parameters, neglecting the significant influence of aging effects. To address this limitation, this study proposes an adaptive observer for temperature estimation in ASSBs, incorporating time-varying thermal parameters. By introducing adaptability into thermal parameter estimation, this research improves the accuracy of temperature estimation, which is crucial for optimizing battery management strategies and ensuring safe operation throughout the battery's lifespan. The key contributions of this work are:

- Extension of the quintuple thermal model presented in [6], with the development of an adaptive observer tailored to the cascaded quintuple thermal model of ASSBs, enhancing temperature estimation by dynamically adjusting to time-varying thermal parameters.
- To the best of the authors' knowledge, this is the first use of the frozen time approximation to match the characteristic equation of a Linear Time-Varying (LTV) system with that of an adaptive observer. While [7, Chapter 4] suggests constructing an adaptive observer using a nonminimal representation, the challenge of handling a transfer function that varies with adaptive parameters remains. This paper proposes the frozen time approximation to address this, enhancing the identification of thermal conductivity uncertainties for improved thermal management.

The article is organized as follows: Section II presents the electrochemical and quintuple thermal models. Section III introduces the adaptive model. Section IV discusses results, followed by conclusions and future work in Section V.

II. Electrochemical-Thermal Model

The ASSB has a pouch configuration, with its components shown in Figure 1. The anode is metallic lithium, the cathode is $LiCoO_2$, and the electrolyte is amorphous Li_3PO_4, separating the anode and cathode [8]. Subsection II-A describes the electrochemical model used to calculate heat generation, while Subsection II-B covers the quintuple thermal model based on this heat generation.

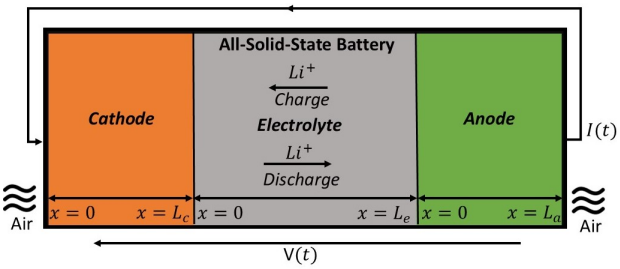

Fig. 1: ASSB schematic.

Assumption 1. *In this study, changes in air temperature $T_{air}(t)$ are neglected.*

P. Ferreira and S.-X. Tang (corresponding author) are with the Department of Mechanical Engineering, Texas Tech University, Lubbock, USA. patferre@ttu.edu, shuxia.tang@ttu.edu.

A. Electrochemical model

The substantial exchange current density for the metallic lithium makes the anode's charge transfer overpotential of anode sufficiently minimal, therefore the anode's charge transfer kinetics are neglected [9]. The concentration of Li^+ ions is regulated by Fick's second law, as described in [10], as follows:

$$\frac{\partial c_{\mathrm{s}}^{-}}{\partial t}(t,x) = D_{\mathrm{s}}^{-}\frac{\partial^2 c_{\mathrm{s}}^{-}}{\partial x^2}(t,x), \quad t>0, \quad x\in(0,L_{\mathrm{c}}), \tag{II.1}$$

$$D_{\mathrm{s}}^{-}\frac{\partial c_{\mathrm{s}}^{-}(t,L_c)}{\partial x} = \frac{I(t)}{FA}, \quad t>0, \quad x\in(0,L_{\mathrm{c}}), \tag{II.2}$$

$$D_{\mathrm{s}}^{-}\frac{\partial c_{\mathrm{s}}^{-}(t,0)}{\partial x} = 0, \quad t>0, \quad x\in(0,L_{\mathrm{c}}), \tag{II.3}$$

$$c_{\mathrm{s}}^{-}(0,x) = c_{\mathrm{s},0}^{-}(x), \quad x\in[0,L_{\mathrm{c}}], \tag{II.4}$$

where c_{s}^{-} is the concentration of Li^+ ions in the cathode, D_{s}^{-} is the diffusion coefficient in the cathode, F is Faraday's constant, A is the cell's cross-sectional area, and $I(t)$ is the applied current in the battery.

The main ionic transport mechanisms in the Li_3PO_4 solid electrolyte are diffusion and migration of Li^+ ions. This process is described by [10]:

$$\frac{\partial c_{\mathrm{e}}}{\partial t}(t,x) = \frac{2D_{\mathrm{Li}}^{+}D_{\mathrm{n}}^{-}}{D_{\mathrm{Li}}^{+}+D_{\mathrm{n}}^{-}}\frac{\partial^2 c_{\mathrm{e}}}{\partial x^2}(t,x) + r(c_{\mathrm{e}}(t,x)), \quad t>0, \quad x\in(0,L_{\mathrm{e}}), \tag{II.5}$$

$$\frac{\partial c_{\mathrm{e}}(t,0)}{\partial x} = -\frac{I(t)}{2FAD_{\mathrm{Li}}^{+}}, \quad t>0, \quad x\in(0,L_{\mathrm{e}}), \tag{II.6}$$

$$\frac{\partial c_{\mathrm{e}}(t,L_e)}{\partial x} = -\frac{I(t)}{2FAD_{\mathrm{Li}}^{+}}, \quad t>0, \quad x\in(0,L_{\mathrm{e}}), \tag{II.7}$$

$$c_{\mathrm{e}}(0,x) = \delta c_{\mathrm{e},0}(x), \quad x\in[0,L_{\mathrm{e}}], \tag{II.8}$$

where c_{e} is the concentration in the electrolyte, D_{Li}^{+} and D_{n}^{-} are diffusion coefficients of Li^+ ions and n^- in the solid electrolyte, δ is the fraction of free Li^+ ions in equilibrium, and r represents the net charge carrier generation.

The charge transfer overpotential $\eta_{\mathrm{ct}}(t)$, the mass transfer overpotential $\eta_{\mathrm{mt}}(t)$ caused by the flow of Li^+ ions in the solid-state electrolyte, and the diffusion overpotential $\eta_{\mathrm{d}}(t)$ at the intercalation electrode interface combine to form the battery's total overpotential, denoted by [6]:

$$\eta_{\mathrm{t}}(t) = \eta_{\mathrm{ct}}(t) + \eta_{\mathrm{mt}}(t) + \eta_{\mathrm{d}}(t). \tag{II.9}$$

A simplified expression for the charge transfer overpotential $\eta_{\mathrm{ct}}(t)$ is given by [6]:

$$\eta_{\mathrm{ct}}(t) = \frac{2RT}{F}\sinh\left(\frac{-I(t)}{2i_{0,\mathrm{pos}}(t)}\right), \tag{II.10}$$

where the exchange current density $i_{0,\mathrm{pos}}(t)$, which depends on the Li^+ ions concentration in $LiCoO_2$ at the electrolyte-cathode interface, is given by [6]:

$$i_{0,\mathrm{pos}}(t) = FAk_{\mathrm{pos}}\left(\frac{(c_{\mathrm{s,max}}^{-}-c_{\mathrm{s}}^{-}(L_e,t))c_{\mathrm{e}}(L_e,t)}{(c_{\mathrm{s,max}}^{-}-c_{\mathrm{min}}^{-})c_{\mathrm{s},0}}\right)^{\alpha_{\mathrm{pos}}} \times\left(\frac{(c_{\mathrm{s}}^{-}(L_e,t)-c_{\mathrm{s,min}}^{-})}{(c_{\mathrm{s,max}}^{-}-c_{\mathrm{s,min}}^{-})}\right)^{1-\alpha_{\mathrm{pos}}}, \tag{II.11}$$

where $c_{\mathrm{s,max}}^{-}$ is the maximum concentration in the cathode and $c_{\mathrm{s,min}}^{-}$ is the minium concentration in cathode. The mass transfer overpotential $\eta_{\mathrm{mt}}(t)$ and the diffusion overpotential $\eta_{\mathrm{d}}(t)$ are given by [6] as follows:

$$\eta_{\mathrm{mt}}(t) = \frac{L_eRTI(t)}{c_{\mathrm{Li}}^{+}F^2A(D_{\mathrm{Li}}^{+}+D_{\mathrm{n}}^{-})}, \tag{II.12}$$

$$\eta_{\mathrm{d}}(t) = E_{\mathrm{eq}}(\theta_s(t)) - E_{\mathrm{eq}}(\bar{\theta}_s(t)), \tag{II.13}$$

where E_{eq} is the equilibrium potential in the cathode [10].

The terminal voltage is given by:

$$V(t) = E_{\mathrm{eq}}(\bar{\theta}_s(t)) + \eta_{\mathrm{t}}(t). \tag{II.14}$$

The product of current and voltage defines the electrochemical heat generation, $S(t)$, representing the energy dissipated as heat [11, Chapter 1, Section 1.4.1]. The expression for heat generation is:

$$S(t) = V(t)|I(t)|, \tag{II.15}$$

where $I(t)$ is the current input and $V(t)$ is the voltage output. The inclusion of the absolute value, $|I(t)|$, guarantees that the thermal power remains positive, since heat generation is inherently a positive quantity [12, Chapter 2, Section 2.1], irrespective of whether the current represents charging or discharging.

B. Quintuple Thermal Model

A thermal model for ASSBs, shown in Fig. 1, was proposed in [6], incorporating five temperature states: the left cathode boundary, cathode, solid electrolyte, anode, and right anode boundary. The model accounts for electrochemical heat from Li^+ ion movement and heat conduction via thermal resistances. Accurate thermal conductivity of the cathode, electrolyte, and anode is essential for efficient heat transfer. Since thermal conductivity degrades over time due to structural changes and environmental conditions [13], it is modeled as time-dependent, with $k_{\mathrm{c}}(t)$, $k_{\mathrm{e}}(t)$, and $k_{\mathrm{a}}(t)$ representing these variations.

The state-space representation of the model for the ASSB, under Assumption 1 and with adaptive thermal conductivities, is given by:

$$\dot{\boldsymbol{T}}(t) = \mathcal{A}(t)\boldsymbol{T}(t) + \boldsymbol{b}u(t), \tag{II.16}$$

$$y(t) = \boldsymbol{c}^{\mathrm{tr}}\boldsymbol{T}(t), \tag{II.17}$$

where

$$\mathbf{T}(t) = \begin{bmatrix} T_{\mathrm{s}^-}(t) & T_{\mathrm{c}}(t) & T_{\mathrm{e}}(t) & T_{\mathrm{a}}(t) & T_{\mathrm{s}^+}(t) \end{bmatrix}^{\mathrm{tr}}, \tag{II.18}$$

$$\mathcal{A}(t) = \begin{bmatrix} -\alpha_1 - \beta_1(t) & \beta_1(t) & 0 & 0 & 0 \\ \beta_2(t) & -\beta_2(t) & 0 & 0 & 0 \\ 0 & \beta_3(t) & -\beta_3(t) & 0 & 0 \\ 0 & 0 & \beta_4(t) & -\beta_4(t) & 0 \\ 0 & 0 & 0 & \beta_5(t) & -\beta_5(t) + \alpha_1 \end{bmatrix}, \tag{II.19}$$

$$\boldsymbol{b} = \begin{bmatrix} 0 & \frac{1}{\lambda_{\mathrm{c}}} & \frac{1}{\lambda_{\mathrm{e}}} & \frac{1}{\lambda_{\mathrm{a}}} & 0 \end{bmatrix}^{\mathrm{tr}}, \tag{II.20}$$

$$u(t) = S(t), \tag{II.21}$$

$$\boldsymbol{c} = \begin{bmatrix} 0 & 0 & 0 & 0 & 1 \end{bmatrix}^{\mathrm{tr}}. \tag{II.22}$$

The notations $\mathrm{s}^-, \mathrm{c}, \mathrm{e}, \mathrm{a}, \mathrm{s}^+$ refer to the left boundary of the cathode, the cathode, the electrolyte, the anode, and the right boundary of the anode, as illustrated in Figure 1. The state vector $\boldsymbol{T}(t)$ represents the system temperatures, $u(t)$ is the input, and $S(t)$ corresponds to the electrochemical heat generation as described in Subsection II-A. The parameters in equation (II.19) are defined as follows:

$$\alpha_1 = \frac{1}{\lambda_{\mathrm{air}} R_{\mathrm{air}}}, \qquad \beta_1(t) = \frac{(k_{\mathrm{c}} + \Delta k_c(t))\, A_c}{\lambda_{\mathrm{air}} L_{\mathrm{c}}},$$
$$\beta_2(t) = \frac{(k_{\mathrm{c}} + \Delta k_c(t))\, A_c}{\lambda_{\mathrm{c}} L_{\mathrm{c}}}, \quad \beta_3(t) = \frac{(k_{\mathrm{e}} + \Delta k_e(t))\, A_e}{\lambda_{\mathrm{e}} L_{\mathrm{e}}},$$
$$\beta_4(t) = \frac{(k_{\mathrm{e}} + \Delta k_e(t))\, A_e}{\lambda_{\mathrm{a}} L_{\mathrm{e}}}, \quad \beta_5(t) = \frac{(k_{\mathrm{a}} + \Delta k_a(t))\, A_a}{\lambda_{\mathrm{air}} L_{\mathrm{a}}},$$

where $\lambda_i = v_i \rho_i c_{p_i}$ represents the product of volume, density, and heat capacity for $i \in \{\mathrm{air}, \mathrm{c}, \mathrm{e}, \mathrm{a}\}$, and the thermal conductivities are given by k_{c}, k_{e}, and k_{a}. The uncertainties in these thermal conductivities are represented by $\Delta k_{\mathrm{c}}(t)$, $\Delta k_{\mathrm{e}}(t)$, and $\Delta k_{\mathrm{a}}(t)$.

III. Adaptive Observer for Temperature Estimation in ASSB

In this section, the adaptive update law for parameters is developed to update the thermal conductivities in the system (II.16)–(II.17), based on which the adaptive Luenberger observer for temperature estimation is designed.

Assumption 2. *For any time instant $t \in [0, \infty)$, the pair $(\mathcal{A}(t), \boldsymbol{c})$ is observable.*

Following Assumption 2, the single-input-single-output system (II.16)-(II.17) can be represented as [7, Chapter 4, Section 4.3]:

$$\dot{y}(t) = -\lambda y(t) + \boldsymbol{\theta}^{\mathrm{tr}} \boldsymbol{\omega}(t), \tag{III.1}$$
$$\dot{\boldsymbol{\omega}}_1(t) = \Lambda \boldsymbol{\omega}_1(t) + \boldsymbol{\psi} u(t), \tag{III.2}$$
$$y_1(t) = \boldsymbol{c}^{\mathrm{tr}} \boldsymbol{\omega_1}(t) + c_0 u(t), \tag{III.3}$$
$$\dot{\boldsymbol{\omega}}_2(t) = \Lambda \boldsymbol{\omega}_2(t) + \boldsymbol{\psi} y(t), \tag{III.4}$$
$$y_2(t) = \boldsymbol{d}^{\mathrm{tr}} \boldsymbol{\omega_2}(t) + d_0 y(t), \tag{III.5}$$

where $\lambda > 0$ is an arbitrarily chosen scalar, $\mathbf{c} \in \mathbb{R}^{4\times 1}$, $c_0 \in \mathbb{R}$, $\mathbf{d} \in \mathbb{R}^{4\times 1}$, and $d_0 \in \mathbb{R}$ are unknown parameters. $\boldsymbol{\omega}_1 \in \mathbb{R}^{4\times 1}$ and $\boldsymbol{\omega}_2 \in \mathbb{R}^{4\times 1}$ are auxiliary states. Here,

$$\Lambda = \begin{bmatrix} -\alpha_1 - \beta_1 & \beta_1 & 0 & 0 \\ \beta_2 & -\beta_2 & 0 & 0 \\ 0 & \beta_3 & -\beta_3 & 0 \\ 0 & 0 & \beta_4 & -\beta_4 \end{bmatrix}, \tag{III.6}$$

$$\boldsymbol{\psi} = \begin{bmatrix} 0 & \frac{1}{\lambda_{\mathrm{c}}} & \frac{1}{\lambda_{\mathrm{e}}} & \frac{1}{\lambda_{\mathrm{a}}} \end{bmatrix}^{\mathrm{tr}}, \tag{III.7}$$

$$\boldsymbol{\omega}(t) \triangleq \begin{bmatrix} u(t) & \boldsymbol{\omega}_1^{\mathrm{tr}}(t) & y(t) & \boldsymbol{\omega}_2^{\mathrm{tr}}(t) \end{bmatrix}^{\mathrm{tr}} \in \mathbb{R}^{10\times 1}. \tag{III.8}$$

The parameter vector is given by:

$$\boldsymbol{\theta} \triangleq \begin{bmatrix} c_0 & \boldsymbol{c}^{\mathrm{tr}} & d_0 & \boldsymbol{d}^{\mathrm{tr}} \end{bmatrix}^{\mathrm{tr}} \in \mathbb{R}^{10\times 1}. \tag{III.9}$$

Applying the Laplace transform to Equation (III.2), $\boldsymbol{W}_1(s)$ is given by:

$$s\boldsymbol{W}_1(s) = \Lambda \boldsymbol{W}_1(s) + \boldsymbol{\psi} U(s),$$
$$\boldsymbol{W}_1(s) = (sI - \Lambda)^{-1} \boldsymbol{\psi} U(s). \tag{III.10}$$

Similarly, applying the Laplace transform to Equation (III.4), we get:

$$s\boldsymbol{W}_2(s) = \Lambda \boldsymbol{W}_2(s) + \boldsymbol{\psi} Y(s),$$
$$\boldsymbol{W}_2(s) = (sI - \Lambda)^{-1} \boldsymbol{\psi} Y(s). \tag{III.11}$$

A. Adaptive Update Law for Thermal Conductivity Estimation

The objective is to determine the parameters c_0, $\boldsymbol{c}$, d_0, $\boldsymbol{d}$, and λ such that the system (III.1)-(III.5) maintains the same transfer function as the original system (II.16)-(II.17). An adaptive update law is to be designed, following the methodology in [7, Chapter 4, Section 4.3], to estimate $\boldsymbol{\theta}$.

In the LTV case, obtaining a transfer function is challenging for $t \in [0, \infty)$ due to the time-dependent nature of system parameters. To address this, the system is discretized using the frozen-time approximation [14], which allows it to be treated time-invariant system within each interval.

Assumption 3. *In each interval $t \in [t_i, t_{i+1})$, $i \in \mathbb{N}$, the frozen-time approximation assumes that the thermal conductivities remain constant, i.e., $\Delta k_c(t) = \Delta k_c(t_i)$, $\Delta k_e(t) = \Delta k_e(t_i)$, and $\Delta k_a(t) = \Delta k_a(t_i)$.*

As a result, the system matrix $\mathcal{A}(t)$ is approximated as $\mathcal{A}(t_i)$. Thus, the system's transfer function in each time interval $[t_i, t_{i+1})$, for $i \in \mathbb{N}$, is given by:

$$G_i(s) = \boldsymbol{c} \left(sI - \mathcal{A}(t_i)\right)^{-1} \boldsymbol{b}. \tag{III.12}$$

For $t \in [t_i, t_{i+1}), i \in \mathbb{N}$, design an adaptive observer for the system (III.1)–(III.5) as

$$\dot{\hat{y}}(t) = -\lambda \hat{y}(t) + \hat{\boldsymbol{\theta}}^{\mathrm{tr}}(t_i) \hat{\boldsymbol{\omega}}(t), \tag{III.13}$$
$$\dot{\hat{\boldsymbol{\omega}}}_1(t) = \Lambda \hat{\boldsymbol{\omega}}_1(t) + \boldsymbol{\psi} u(t), \tag{III.14}$$
$$\hat{y}_1(t) = \hat{\boldsymbol{c}}^{\mathrm{tr}}(t_i) \hat{\boldsymbol{\omega}}_{\boldsymbol{1}}(t) + \hat{c}_0(t_i) u(t), \tag{III.15}$$
$$\dot{\hat{\boldsymbol{\omega}}}_2(t) = \Lambda \hat{\boldsymbol{\omega}}_2(t) + \boldsymbol{\psi} y(t), \tag{III.16}$$
$$\hat{y}_2(t) = \hat{\boldsymbol{d}}^{\mathrm{tr}}(t_i) \hat{\boldsymbol{\omega}}_{\boldsymbol{2}}(t) + \hat{d}_0(t_i) y(t), \tag{III.17}$$
$$\hat{y}(t) = \hat{T}_s^+(t), \tag{III.18}$$

where $\hat{\boldsymbol{\theta}}(t)$ is the estimated parameter vector for (III.9). For all $t \in [t_i, t_{i+1})$, the estimated parameter vector $\hat{\boldsymbol{\theta}}(t)$ based on the frozen-time approximation is expressed as:

$$\hat{\boldsymbol{\theta}}(t) = \begin{bmatrix} \hat{c}_0(t_i) & \hat{\boldsymbol{c}}^{\text{tr}}(t_i) & \hat{d}_0(t_i) & \hat{\boldsymbol{d}}^{\text{tr}}(t_i) \end{bmatrix}^{\text{tr}} \in \mathbb{R}^{10\times 1}, \tag{III.19}$$

and $\hat{\boldsymbol{\omega}}(t)$ is the estimate from (III.8), defined as:

$$\hat{\boldsymbol{\omega}}(t) = \begin{bmatrix} u(t) & \hat{\boldsymbol{\omega}}_1^{\text{tr}}(t) & y(t) & \hat{\boldsymbol{\omega}}_2^{\text{tr}}(t) \end{bmatrix}^{\text{tr}} \in \mathbb{R}^{10\times 1}. \tag{III.20}$$

The adaptive update law for updating the parameter vector is given by:

$$\dot{\hat{\boldsymbol{\theta}}}(t) = -\left(\hat{y}(t) - y(t)\right)\hat{\boldsymbol{\omega}}(t), \quad \forall t \in [t_i, t_{i+1}). \tag{III.21}$$

Without loss of generality, assuming all zero initial conditions, $\hat{\boldsymbol{W}}_1(s)$ is given by:

$$\hat{\boldsymbol{W}}_1(s) = (sI - \Lambda)^{-1}\boldsymbol{\psi}U(s). \tag{III.22}$$

For $t \in [t_i, t_{i+1})$, the output $\hat{Y}_{1,i}(s)$ is expressed as:

$$\hat{Y}_{1,i}(s) = \hat{\boldsymbol{c}}^{\text{tr}}(t_i)\hat{\boldsymbol{W}}_1(s) + \hat{c}_0(t_i)U(s). \tag{III.23}$$

By applying (III.22), the transfer function $\hat{G}_{1,i}(s)$ associated with $\hat{\boldsymbol{\omega}}_1(s)$ for $t \in [t_i, t_{i+1})$ is given by:

$$\hat{G}_{1,i}(s) = \frac{\hat{Y}_{1,i}(s)}{U(s)} = \hat{\boldsymbol{c}}^{\text{tr}}(t_i)(sI - \Lambda)^{-1}\boldsymbol{\psi} + \hat{c}_0(t_i). \tag{III.24}$$

Similarly, $\hat{\boldsymbol{W}}_2(s)$ is given by:

$$\hat{\boldsymbol{W}}_2(s) = (sI - \Lambda)^{-1}\boldsymbol{\psi}Y(s). \tag{III.25}$$

For $t \in [t_i, t_{i+1})$, the output $\hat{Y}_2(s)$ is given by:

$$\hat{Y}_{2,i}(s) = \hat{\boldsymbol{d}}^{\text{tr}}(t_i)\hat{\boldsymbol{W}}_2(s) + \hat{d}_0(t_i)Y(s). \tag{III.26}$$

By applying (III.25), the transfer function $\hat{G}_{2,i}(s)$ associated with (III.16) for $t \in [t_i, t_{i+1})$ is expressed as:

$$\hat{G}_{2,i}(s) = \frac{\hat{Y}_{2,i}(s)}{Y(s)} = \hat{\boldsymbol{d}}^{\text{tr}}(t_i)(sI - \Lambda)^{-1}\boldsymbol{\psi} + \hat{d}_0(t_i). \tag{III.27}$$

For (III.13), the following expression is derived:

$$s\hat{Y}_i(s) = -\lambda\hat{Y}_i(s) + \hat{\boldsymbol{\theta}}^{\text{tr}}(t_i)\hat{\boldsymbol{W}}(s), \tag{III.28}$$

then, the output $\hat{Y}_i(s)$ for $t \in [t_i, t_{i+1})$ becomes:

$$\hat{Y}_i(s) = \frac{\hat{\boldsymbol{\theta}}^{\text{tr}}(t_i)\hat{\boldsymbol{W}}(s)}{s + \lambda}. \tag{III.29}$$

By combining the transfer functions in Equations (III.29), (III.24), and (III.27), the transfer function relating the input to the output of the system described by Equations (III.13)–(III.18) for $t \in [t_i, t_{i+1})$ is expressed as follows:

$$\hat{W}_i(s) = \frac{\hat{P}_i(s)}{(s + \lambda)R(s) - \hat{Q}_i(s)}, \tag{III.30}$$

where

$$\hat{P}_i(s) \triangleq \hat{\boldsymbol{c}}^{\text{tr}}(t_i)(sI - \Lambda)^{-1}\boldsymbol{\psi} + \hat{c}_0(t_i), \tag{III.31}$$

$$\hat{Q}_i(s) \triangleq \hat{\boldsymbol{d}}^{\text{tr}}(t_i)(sI - \Lambda)^{-1}\boldsymbol{\psi} + \hat{d}_0(t_i), \tag{III.32}$$

$$R(s) \triangleq \det(sI - \Lambda). \tag{III.33}$$

The parameters $\hat{c}_0(t_i), \hat{\boldsymbol{c}}^{\text{tr}}(t_i), \hat{d}_0(t_i), \hat{\boldsymbol{d}}^{\text{tr}}(t_i)$ are updated at each interval, causing the transfer function to evolve over time.

Note that $\hat{\boldsymbol{W}}_1(s)$ and $\hat{\boldsymbol{W}}_2(s)$ are the Laplace transform of $\hat{\boldsymbol{\omega}}_1(t)$ and $\hat{\boldsymbol{\omega}}_2(t)$ in the system (III.13)-(III.18), while $\hat{W}_i(s), i \in \mathbb{N}$ represents the transfer function of the system (III.13)-(III.18) for each time interval $[t_i, t_{i+1})$.

The following theorem holds.

Theorem 1. *Consider the system* (III.1)-(III.5) *for* $t \in [0, \infty)$ *with initial conditions* $\mathbf{T}(0)$ *and* $\hat{\mathbf{T}}(0)$*, and an input* $u(t)$*. For each interval* $t \in [t_i, t_{i+1})$, $i \in \mathbb{N}$*, define the adaptive observer* (III.13)-(III.18)*, where the parameter vector* $\hat{\boldsymbol{\theta}}(t)$ *is updated according to the adaptive update law* (III.21)*. Then, the estimated parameter vector* $\hat{\boldsymbol{\theta}}(t)$ *converges to the true parameter vector* $\boldsymbol{\theta}$ *as* $t \to \infty$*.*

Proof. The output error and parameter error are defined as:

$$e(t) \triangleq \hat{y}(t) - y(t), \tag{III.34}$$

$$\tilde{\boldsymbol{\theta}}(t) \triangleq \hat{\boldsymbol{\theta}}(t) - \boldsymbol{\theta}. \tag{III.35}$$

As a result,

$$\dot{e}(t) = -\lambda e(t) + \tilde{\boldsymbol{\theta}}^{\text{tr}}(t_i)\hat{\boldsymbol{\omega}}(t) + \boldsymbol{\theta}^{\text{tr}}\tilde{\boldsymbol{\omega}}(t). \tag{III.36}$$

For a positive definite matrix Q, P is the unique symmetric positive definite matrix such that $\Lambda^T P + P\Lambda = -Q < 0$. For each interval $t \in [t_i, t_{i+1})$, $i \in \mathbb{N}$, the Lyapunov function is defined as:

$$V_i(e(t), \tilde{\boldsymbol{\theta}}(t), \tilde{\boldsymbol{\omega}}(t)) = \frac{1}{2}\left(e^2(t) + \tilde{\boldsymbol{\theta}}^{\text{tr}}(t_i)\tilde{\boldsymbol{\theta}}(t) + \beta\tilde{\boldsymbol{\omega}}^{\text{tr}}(t)P\tilde{\boldsymbol{\omega}}(t)\right), \tag{III.37}$$

where β is a positive scalar constant to be chosen. Applying the adaptive law (III.21) for $t \in [t_i, t_{i+1})$, $i \in \mathbb{N}$, gives

$$\dot{V}_i(e(t), \tilde{\boldsymbol{\theta}}(t), \tilde{\boldsymbol{\omega}}(t)) = -\lambda e^2(t) + e(t)\boldsymbol{\theta}^{\text{tr}}\tilde{\boldsymbol{\omega}}(t) - \tilde{\boldsymbol{\theta}}^{\text{tr}}(t)e(t)\hat{\boldsymbol{\omega}}(t). \tag{III.38}$$

Applying Young's inequality to $e(t)\boldsymbol{\theta}^{\text{tr}}\tilde{\boldsymbol{\omega}}(t)$ and Cauchy-Schwarz inequality to $\boldsymbol{\theta}^{\text{tr}}\tilde{\boldsymbol{\omega}}(t)$ gives

$$\dot{V}_i(e(t), \tilde{\boldsymbol{\theta}}(t), \tilde{\boldsymbol{\omega}}(t)) \leq -\frac{3\lambda}{4}e^2(t) + \left(\frac{\|\boldsymbol{\theta}\|^2}{\lambda} - \frac{\beta}{2}\lambda_{\min}(Q)\right)\|\tilde{\boldsymbol{\omega}}(t)\|^2, \tag{III.39}$$

where $\lambda_{\min}(Q)$ is the minimum eigenvalue of the matrix Q. Thus, choosing

$$\beta > \frac{2\|\boldsymbol{\theta}\|^2}{\lambda\lambda_{\min}(Q)}, \tag{III.40}$$

ensures that $\dot{V}_i(t) \leq -\frac{3\lambda}{4}e^2(t)$ holds piecewise for $t \in [t_i, t_{i+1}), i \in \mathbb{N}$, guaranteeing uniform stability of the output error piecewise. This further ensures that the origin of the

error system remains uniformly stable for $t \in [0, \infty)$. Moreover, asymptotic stability follows by showing that the output error belongs to $\mathcal{L}^2$ and applying Lemma 2.12 [7, Chapter 2, Section 2.8], as well as using persistent excitation conditions for parameter convergence, as detailed in [7, Chapter 4, Section 4.3]. Due to page limitations, the detailed proof is omitted here. □

B. Adaptive Observer for Temperature Estimation

Using the adaptive update law (III.21), the parameters $\hat{c}_0(t_i)$, $\hat{\boldsymbol{c}}(t_i)$, $\hat{d}_0(t_i)$, and $\hat{\boldsymbol{d}}(t_i)$ are estimated. Since the adaptive observer structure (III.13)-(III.18) is chosen to accurately replicate the dynamics of the original system, as discussed in [7, Chapter 4, Section 4.3], the observer inherently shares the same transfer function with the original system at each time step under the frozen-time approximation (Assumption 3). Specifically, the frozen-time approximation treats the system as locally linear and time-invariant within each interval $[t_i, t_{i+1})$, generating a family of transfer functions with identical structures but varying parameters over time. This allows explicit matching between the observer's transfer function and that of the real system, facilitating the identification of parameter uncertainties. Once the adaptive parameters are estimated, the observer (III.13)-(III.18) updates the system matrix $\hat{\mathcal{A}}(t_i)$, which reflects the estimated thermal conductivity uncertainties, and is given by:

$$\hat{\mathcal{A}}(t_i) = \begin{bmatrix} -\alpha_1 - \hat{\beta}_1(t_i) & \hat{\beta}_1(t_i) & 0 & 0 & 0 \\ \hat{\beta}_2(t_i) & -\hat{\beta}_2(t_i) & 0 & 0 & 0 \\ 0 & \hat{\beta}_3(t_i) & -\hat{\beta}_3(t_i) & 0 & 0 \\ 0 & 0 & \hat{\beta}_4(t_i) & -\hat{\beta}_4(t_i) & 0 \\ 0 & 0 & 0 & \hat{\beta}_5(t_i) & -\hat{\beta}_5(t_i) + \alpha_1 \end{bmatrix}, \tag{III.41}$$

where the estimated parameters are:

$$\hat{\beta}_1(t_i) = \frac{(k_{\mathrm{c}} + \hat{\Delta}k_c(t_i))A_c}{\lambda_{\mathrm{air}} L_{\mathrm{c}}}, \quad \hat{\beta}_2(t_i) = \frac{(k_{\mathrm{c}} + \hat{\Delta}k_c(t_i))A_c}{\lambda_{\mathrm{c}} L_{\mathrm{c}}},$$
$$\hat{\beta}_3(t_i) = \frac{(k_{\mathrm{e}} + \hat{\Delta}k_e(t_i))A_e}{\lambda_{\mathrm{e}} L_{\mathrm{e}}}, \quad \hat{\beta}_4(t_i) = \frac{(k_{\mathrm{e}} + \hat{\Delta}k_e(t_i))A_e}{\lambda_{\mathrm{a}} L_{\mathrm{e}}},$$
$$\hat{\beta}_5(t_i) = \frac{(k_{\mathrm{a}} + \hat{\Delta}k_a(t_i))A_a}{\lambda_{\mathrm{air}} L_{\mathrm{a}}}.$$

The characteristic equations obtained by equating the observer transfer function (III.30) with the original system (II.17) for all $t \in [t_i, t_{i+1})$ is given by:

$$(s + \lambda)\hat{R}(s) - \hat{Q}_i(s) = \det(sI - \hat{\mathcal{A}}(t_i)). \tag{III.42}$$

Matching these characteristic equations allows the identification of the thermal conductivity uncertainties $\hat{\Delta}k_c$, $\hat{\Delta}k_a$, and $\hat{\Delta}k_e$.

Assumption 4. *For any $i \in \mathbb{N}$, the pair $(\hat{\mathcal{A}}(t_i), \boldsymbol{c})$ is observable.*

The Luenberger observer utilizes output errors for state estimation, with temperature estimation for (II.16)-(II.17) following from (III.43), as described in [15]:

$$\dot{\hat{\mathbf{T}}}(t) = \hat{\mathcal{A}}(t_i)\hat{\mathbf{T}}(t) + \mathcal{B}\mathbf{u}(t) + \boldsymbol{l}_i \boldsymbol{c}[\mathbf{T}(t) - \hat{\mathbf{T}}(t)], \tag{III.43}$$

where $\boldsymbol{l}_i$ is the observer gain and should be chosen using Assumption 4.

Theorem 2. *Consider the system* (II.16)-(II.17) *and the observer* (III.43) *for $t \in [t_i, t_{i+1})$, $i \in \mathbb{N}$. The matrix $\tilde{\mathcal{A}}(t_i)$ is updated using the adaptive law* (III.21). *Choose the observer gain $\boldsymbol{L}_i \in \mathbb{R}^{5\times 1}$ such that the matrix $\tilde{\mathcal{A}}(t_i) - \boldsymbol{L}_i\mathcal{C}$ remains Hurwitz for all $t \in [t_i, t_{i+1})$. For any initial conditions $\mathbf{T}(0)$ and $\hat{\mathbf{T}}(0)$, and any input $u(t)$, the observer error $\tilde{\mathbf{T}}(t) = \hat{\mathbf{T}}(t) - \mathbf{T}(t)$ converges exponentially to zero.*

Proof. The proof follows similar arguments as in [16]. Since this holds for every interval $[t_i, t_{i+1})$, it extends to all $t \in [0, \infty)$. Due to page limitations, the full derivation is omitted. □

IV. Simulation Results

Simulations were performed in MATLAB on an MSI PC (Intel i7-13620H, 16 GB RAM). The 5th-order Padé approximation [6] was used to linearize the model, converting the PDE into ODEs. The scalar parameter was chosen as $\lambda = 4.45$, with an initial temperature of 25°C. The original system parameters are $c_0 = 4.59$, $\boldsymbol{c} = [4.59; 4.59; 4.59; 4.59]^{\mathrm{tr}}$, $d_0 = 0.043$, and $\boldsymbol{d} = [0.01; 0.01; 0.01; 0.01]^{\mathrm{tr}}$. The thermal conductivity uncertainties, Δk_c, Δk_e, and Δk_a, were initialized as constants and subsequently updated online by the adaptive observer. The values of electrochemical and thermal properties are taken from [6].

Figure 2 shows the Urban Dynamometer Driving Schedule (UDDS) [17], which was used as input for the electrochemical model.

The 2500s UDDS, with a 1s interval, generated over 2500 transfer functions and characteristic equations for uncertainty analysis.

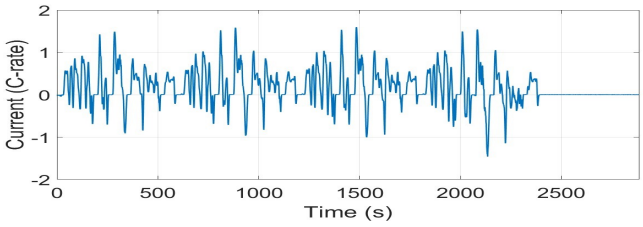

Fig. 2: Urban Dynamometer Driving Schedule (UDDS).

Figure 3 shows the evolution of thermal conductivities. The solid blue lines represent the adaptive conductivities $\hat{k}_c$, $\hat{k}_e$, and $\hat{k}_a$, while the red dashed lines show the reference values. $\hat{k}_c$ remains close to the reference, $\hat{k}_e$ varies more due to thermal changes, and $\hat{k}_a$ initially fluctuates but stabilizes. These results demonstrate the observer's effectiveness in tracking time-varying properties.

Figure 4 shows the temperatures $\hat{T}_{\mathrm{s}}^{-}$, $\hat{T}_{\mathrm{c}}$, $\hat{T}_{\mathrm{e}}$, $\hat{T}_{\mathrm{a}}$, and $\hat{T}_{\mathrm{s}}^{+}$, based on thermal conductivity estimation. The temperatures rise and stabilize over time. Between 2200 and 2300 seconds, they are nearly steady, as internal heat generation ceases after the current drops to zero (Figure 2).

Figure 5 illustrates the error dynamics between the Luenberger observer and the real system. The graph shows significant initial errors due to different starting conditions. However, the errors for all temperatures converge to zero,

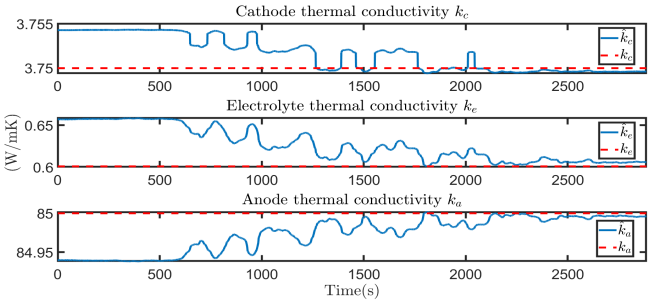

Fig. 3: Thermal conductivity estimation.

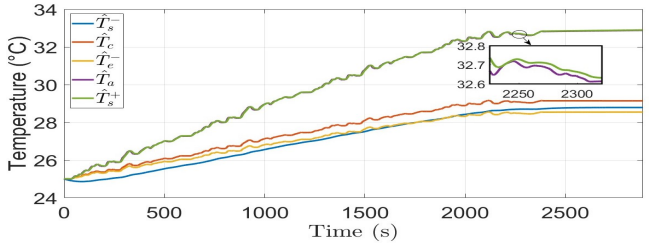

Fig. 4: Temperature estimation $\hat{\boldsymbol{T}}$.

indicating that the observer is accurately tracking the real system's temperatures. The zoomed-in section highlights the immediate differences during the first few seconds of the simulation, emphasizing the initial discrepancies between the observer and the real system.

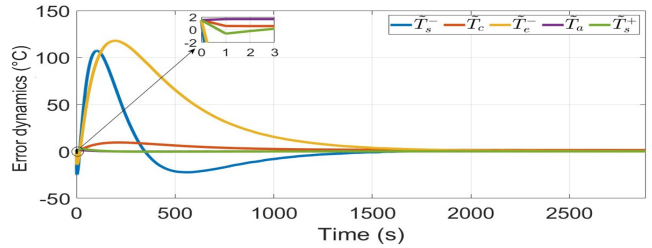

Fig. 5: Observer error $\tilde{\boldsymbol{T}}(t)$, the difference between estimated $\hat{\mathbf{T}}(t)$ and actual temperatures $\mathbf{T}(t)$.

V. Conclusion and Future Work

An adaptive observer for the quintuple thermal model ASSBs was developed, demonstrating effective real-time estimation of both temperatures and time-varying thermal conductivity parameters. By employing a frozen-time approximation, the observer successfully addressed the inherent complexity of the battery's LTV behavior, enabling robust parameter adaptation. Simulation results under the UDDS confirmed that the adaptive observer accurately tracks the battery's thermal behavior, exhibiting rapid parameter convergence and exponential decay of estimation errors. These results highlight the observer's capability to enhance thermal management strategies significantly, thus contributing to safer and more efficient battery operations.

Future research will extend the adaptive framework to incorporate cathode and electrolyte concentration dynamics, further enhancing the accuracy of coupled electrochemical-thermal models. Efforts will also focus on integrating the estimated temperatures directly into the electrochemical model, improving real-time heat generation estimation. Additionally, comparing the proposed adaptive observer with other estimation techniques, such as adaptive Kalman filters.

Acknowledgments

The authors sincerely thank Professor Satadru Dey for discussion on the convergence time shown in Figure 5.

References

[1] Alex M Bates, Yuliya Preger, Loraine Torres-Castro, Katharine L Harrison, Stephen J Harris, and John Hewson. Are solid-state batteries safer than lithium-ion batteries? *Joule*, 6(4):742–755, 2022.

[2] Paul Albertus, Venkataramani Anandan, Chunmei Ban, Nitash Balsara, Ilias Belharouak, Josh Buettner-Garrett, Zonghai Chen, Claus Daniel, Marca Doeff, Nancy J Dudney, et al. Challenges for and pathways toward li-metal-based all-solid-state batteries, 2021.

[3] Katherine L Jungjohann, Renae N Gannon, Subrahmanyam Goriparti, Steven J Randolph, Laura C Merrill, David C Johnson, Kevin R Zavadil, Stephen J Harris, and Katharine L Harrison. Cryogenic laser ablation reveals short-circuit mechanism in lithium metal batteries. *ACS Energy Letters*, 6(6):2138–2144, 2021.

[4] Kookjin Heo, Jonggwan Lee, Jehong Im, Min-Young Kim, Ho-Sung Kim, Docheon Ahn, Jaekook Kim, and Jinsub Lim. A composite cathode material encapsulated by amorphous garnet-type solid electrolyte and self-assembled la 2 (ni 0.5 li 0.5) o 4 nanoparticles for all-solid-state batteries. *Journal of Materials Chemistry A*, 8(43):22893–22906, 2020.

[5] D Danilov, RAH Niessen, and PHL Notten. Modeling all-solid-state li-ion batteries. *Journal of the Electrochemical Society*, 158(3):A215, 2010.

[6] Patryck Ferreira and Shu-Xia Tang. Quintuple thermal model for all-solid-state batteries and temperature estimation through a cascaded thermal-electrochemical model. *IEEE Conference on Control Technology and Applications (CCTA)*, 2024.

[7] Kumpati S Narendra and Anuradha M Annaswamy. *Stable adaptive systems*. Courier Corporation, 2012.

[8] Kushagra Upreti, Isaiah Oyewole, Xianke Lin, and Youngki Kim. On simplification of a solid-state battery model for state estimation. In *2019 IEEE Conference on Control Technology and Applications (CCTA)*, pages 487–492. IEEE, 2019.

[9] Dong Zhang, Shu-Xia Tang, Luis D. Couto, and Venkatasubramanian Viswanathan. PDE observer for all-solid-state batteries via an electrochemical model. In *2021 IEEE Conference on Control Technology and Applications (CCTA)*, pages 51–56, 2021.

[10] Zhongwei Deng, Xiaosong Hu, Xianke Lin, Le Xu, Jiacheng Li, and Wenchao Guo. A reduced-order electrochemical model for all-solid-state batteries. *IEEE Transactions on Transportation Electrification*, 7(2):464–473, 2020.

[11] Alexandra Von Meier. *Electric power systems: a conceptual introduction*. John Wiley & Sons, 2006.

[12] Cengel Ya, A Ghajar, and H Ma. Heat and mass transfer fundamentals & applications. *McGraw-Hill*, 2015.

[13] Georgi Kovachev, Andrea Astner, Gregor Gstrein, Luigi Aiello, Johann Hemmer, Wolfgang Sinz, and Christian Ellersdorfer. Thermal conductivity in aged li-ion cells under various compression conditions and state-of-charge. *Batteries*, 7(3):42, 2021.

[14] SD Peters and MM Fahmy. Synthesis of recursive ltv digital filters using the frozen-time approximation. *IEEE transactions on circuits and systems*, 36(3):448–451, 1989.

[15] Robert L Williams, Douglas A Lawrence, et al. *Linear state-space control systems*. John Wiley & Sons, 2007.

[16] Patryck Ferreira and Shu-Xia Tang. Sensors placement analysis and temperature estimation in lithium-ion batteries with a cascaded electrochemical-thermal model. In *2024 European Control Conference (ECC)*, pages 200–205, 2024.

[17] Scott J Moura, Federico Bribiesca Argomedo, Reinhardt Klein, Anahita Mirtabatabaei, and Miroslav Krstic. Battery state estimation for a single particle model with electrolyte dynamics. *IEEE Transactions on Control Systems Technology*, 25(2):453–468, 2016.